CrossMark

A comprehensive semi-analytical model of the polysilicon emitter contact in bipolar transistors

A. Zekry[1] · A. Shaker[2] · M. Ossaimee[2] · M. S. Salem[3,4] · M. Abouelatta[1]

Abstract This paper aims to develop a comprehensive physical model for a bipolar transistor's polysilicon-contacted emitter. Poisson's equation is solved numerically in the emitter–base space charge region to specify the boundary conditions and the excess minority carriers injected from base to emitter. The continuity and current transport equations are also solved numerically to obtain the minority carrier current in the emitter region. The polysilicon along with the interface layers is modeled by using an effective value for the lifetime. In this model, all the technological parameters of different emitter regions are taken into consideration. Also, the heavy doping effects and the built-in electric field in the shallow non-homogeneous doped single crystalline layer are also included. Such a systematic model does not exist in the literature. The results of the analytical model are numerically evaluated using MATLAB. The trends provided by the model are validated against published experimental results whenever possible and found to be in good agreement with them.

Keywords Modeling · Bipolar transistor · Polysilicon emitter contact · Integrated circuit · MATLAB

✉ M. Abouelatta
m.abouelatta@eng.asu.edu.eg

1 Department of Electronics and Communication Engineering, Faculty of Engineering, Ain Shams University, Cairo 11517, Egypt

2 Department of Engineering Physics and Mathematics, Faculty of Engineering, Ain Shams University, Cairo 11517, Egypt

3 Department of Electrical Communication and Electronics Systems Engineering, Faculty of Engineering, Modern Science and Arts University, Cairo, Egypt

4 Department of Computer Engineering, Computer College, Hail University, Hail, Kingdom of Saudi Arabia

1 Introduction

In developing bipolar transistors for integrated circuits, it is required to reduce the transistor area to increase its current amplification factor and the switching speed [1–3]. The major characterization parameters of integrated circuit bipolar transistors include the cross-sectional area of the emitter–base junction (A_E), the saturation current (I_o), the early voltage (V_A), the base transit time (τ_F), the base–emitter zero-bias junction capacitance (C_{je0}) and the base–collector junction capacitance ($C_{\mu0}$) [4,5]. A polysilicon emitter contact improves the BJT current gain, while the transistor speed is not affected by such improvement [6,7]. So, the addition of a polysilicon layer to the single thin crystalline layer enhances its performance significantly [8–11]. Thus, the polysilicon emitter transistors are widely used in high-speed bipolar circuits, contemporary bipolar and BiCMOS IC because of their pronounced features [12,13]. Additionally, these types of contacts has gained attraction in the fabrication of solar cell structures [14].

They have higher current gain and high performance-to-cost ratio compared to the metal contact transistors [15,16]. This high gain, according to the transport theory, is achieved due to low mobility of holes in polysilicon emitter contacts [17]. Because of the complicated structure of the polysilicon emitter, there is no adequate model to explain the electronic phenomena associated with it.

In the literature, many theoretical models have been proposed to investigate the current gain in polysilicon emitter transistors. Some models include the potential barrier model due to the doping atoms segregation at the polysilicon/silicon interface [18,19]. Other models include the mobility reduction model at the grain boundaries in the polysilicon and at the pseudo-grain boundary at the polysilicon/silicon interface [9,20]. Also, the oxide tunneling model, which explains

the improved gain by tunneling through a thin oxide layer at the polysilicon/silicon interface, is also presented [8,21]. Moreover, an analytical model that simulates the current gain improvement of polysilicon emitter bipolar transistors based on the effective recombination velocity method was built [22].

In most cases, the recombination in the single-crystal emitter was neglected [8,9,23,24]. In other situations, a simplified model for the transport in the polysilicon was assumed [25,26]. Furthermore, the grain boundaries were merely considered to be parallel to the n–p junction [21,27,28]. There are a lot of available models that take the effective recombination velocity into consideration. This, in most cases, gives results based only on fitting that may be unphysical.

The emitter consists of a single crystalline layer followed by a polysilicon layer. Between these two layers, there is an interface region (i-layer) which depends greatly on the polysilicon deposition conditions and the surface of emitter before deposition. The structure and physical properties of this i-layer are governing the electrical performance of the polysilicon emitter. Because this layer is thin and has another energy gap than silicon, it is modeled by a potential energy barrier in addition to a Gaussian distribution of recombination centers.

In this work, a mathematical model has been developed. The semiconductor equations have been applied to the different regions of the emitter. The non-homogenous doping profile is taken into consideration as well as the high doping effects on the energy gap and lifetime and the impact of the grain boundaries in the polysilicon region. Moreover, Poisson's equation is solved numerically in the emitter–base space charge region to specify the boundary conditions and the excess minority carriers injected from base to emitter. The continuity and current transport equations are also solved numerically to obtain the minority carrier current in the emitter region. By solving these equations, the I–V characteristic of the emitter is obtained. A simulation program is developed under MATLAB environment to calculate the minority carrier current for any technological parameters. The developed model results are found to be in agreement with the published experimental results. This agreement gives a real validation of the presented model.

2 Description of the emitter region

Bipolar junction transistor (BJT) consists of three regions: the emitter, the base and the collector. The base–collector region must be short-circuited to be able to get the I–V characteristic of the emitter region. The schematic describing such condition is shown in Fig. 1.

When the emitter–base junction is forward biased, the back-injected emitter current determines the injection effi-
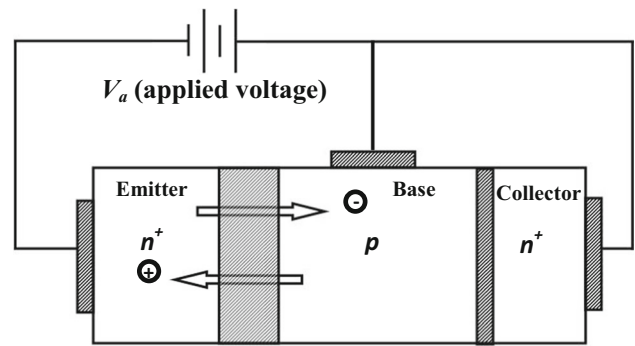
Fig. 1 A typical BJT with shorted collector–base junction

ciency of the emitter and the current amplification factor of the transistor. The base is a p-type material with background acceptor concentration N_A. The emitter region is divided into three layers. The first layer is made of single crystalline silicon with donor doping concentration N_D. The second layer is made of polycrystalline silicon with a particular donor concentration. The third layer is formed at the interface between single and poly-layers. This layer consists of an oxide, insulator, assuming the layer is very thin ($\approx 20 - 30$ Å). This layer could be intentionally grown on the silicon substrate prior to the polysilicon deposition [29]. Meanwhile, it could be found due to any oxide contamination and, in this case, it is called native oxide [28].

Figure 2a shows the different layers of the emitter region: the poly-layer, the SiO$_2$ interface layer and the single crystalline emitter layer. In Fig. 2b, the corresponding energy band diagram of the emitter layers is introduced labeling the relevant material parameters. The interface (SiO$_2$) is very thin. This construction is expected to improve the emitter characteristics and hence the transistor performance.

In practice, the donor impurity distribution ($N_D(x)$) of the single layer is not homogeneous, and it may follow a complementary error function or a Gaussian function as given by Eqs. (1) and (2):

$$N_D(x) = N_s \mathrm{erfc}\left(\frac{x}{2\sqrt{Dt}}\right) \tag{1}$$

$$N_D(x) = N_S e^{-(x/x_l)^2} \tag{2}$$

where N_S is the surface concentration, D is the diffusivity coefficient (cm^2/s), t is the diffusion time, and x_l ($x_l = 2\sqrt{Dt}$) is the characteristic length of the Gaussian function. Equations (1) and (2) are examples of the doping profiles of donor distribution throughout the emitter and hence the pattern of majority carrier concentration (which is, in this case, electrons).

Figure 3 shows the complementary error function as an example. It is clear that with increasing the distance inside the material, the donor concentration N_D decreases until it
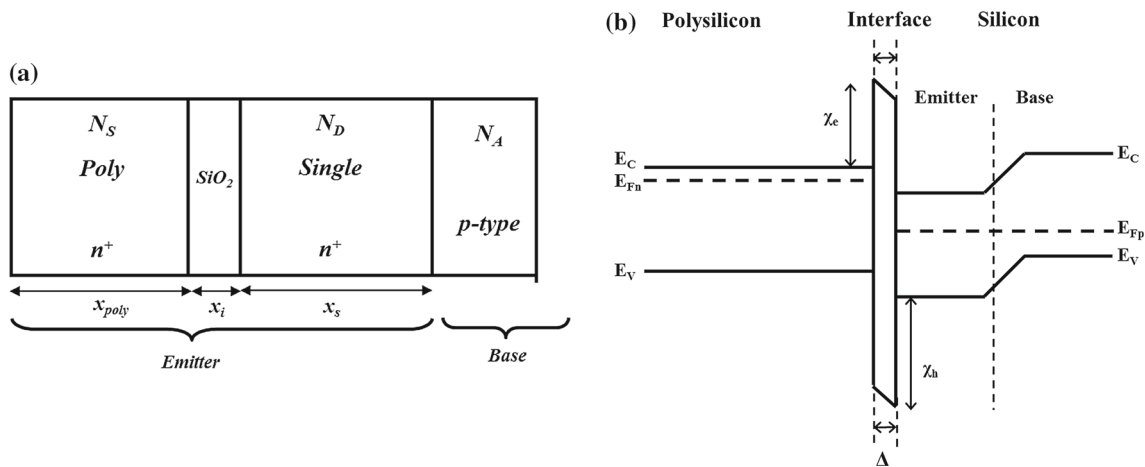
Fig. 2 Emitter region showing **a** emitter layers and the corresponding, **b** energy band diagram
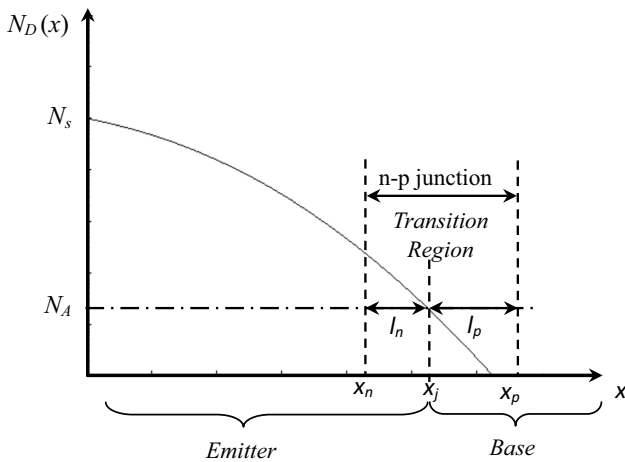
Fig. 3 Profile of the donor and the transition region of the emitter–base junction

reaches the value of background concentration N_A. The point at which ($N_D = N_A$) is the interface between emitter and base. It is called the junction point x_j as indicated in the figure. The transition region width is $W_j = l_n + l_p$ (as shown in the figure). In the next sections, Poisson's equation is solved in the emitter–base junction and specify exactly l_n and l_p and the width of the transition region for certain applied voltage V_a.

3 Transition region calculation

In this section, it is required to determine the excess minority carrier concentration which is not constant for non-homogeneous profiles. Its value changes with the change of the width of the transition region. Thus, its value changes with the applied voltage (V_a). The relation between the applied voltage and l_n and l_p must be obtained to specify the donor

concentration at the edge of the emitter region. According to Boltzmann relation:

$$\Delta p \equiv p(x_n) = p_{no} \left(e^{V_a/V_T} - 1 \right) \tag{3}$$

where p_{no} is the hole concentration at $x = x_n$, i.e.,

$$p_{no} = \frac{n_i^2}{N_D(x_n) - N_A} \tag{4}$$

Now, the physical properties of a p–n junction could be described. Considering the situation in Fig. 3, starting with Poisson's equation,

$$\frac{dE}{dx} = \frac{\rho}{\varepsilon} \tag{5}$$

It is known that $n = p \approx 0$ in the transition region. Furthermore, as the donor concentration is variable with the distance x, the electric field could be written as,

$$E(x) = \int_{x_n}^{x} \frac{qN(x)}{\varepsilon} dx \tag{6}$$

where $x \leq x_j$ and $N(x) = N_D(x) - N_A$. Since the material is neutral around the transition region one has: $E(x_n) = E(x_p) = 0$ then,

$$E(x_p) = \int_{x_n}^{x_j} \frac{qN(x)}{\varepsilon} dx + \int_{x_j}^{x_p} \frac{qN(x)}{\varepsilon} dx = 0 \tag{7}$$

Equation (7) states that for any given value of x_n, one can get the amount of shift toward the base (i.e., l_p) and hence x_p. It is clear that the maximum electric field occurs when $x = x_j$, i.e.,

$$E_{\max} = \int_{x_n}^{x_j} \frac{qN(x)}{\varepsilon} \, dx \qquad (8)$$

The potential at the neutral n-region, emitter region, could be assumed to be equal zero, i.e., $V(x_n) = 0$. As the electric field is known, the potential distribution $V(x)$ could be determined. By definition,

$$\int_{x_n}^{x} dV = \int_{x_n}^{x} E \, dx \qquad (9)$$

Then, the potential at any point x is,

$$V(x) = \int_{x_n}^{x} \left(\int_{x_n}^{x} \frac{qN(x)}{\varepsilon} \, dx \right) dx \qquad (10)$$

Now, the barrier height V_B is defined as

$$V_B = \varphi \mp V_a \qquad (11)$$

The negative sign is for forward bias, and the positive sign is for reverse bias. φ is the built-in voltage defined as the barrier height when no bias is applied, i.e.,

$$\varphi = V_{Bo} \equiv \text{barrier height at } V_a = 0 \qquad (12)$$

The barrier height is a function of x_n at a particular applied voltage, i.e.,

$$V_B = \int_{x_n}^{x_p} E(x) \, dx \qquad (13)$$

At $V_B = \varphi$ (no applied voltage): $x_n = x_{no}$ and $l_n = l_{no}$, then,

$$V_B(x_{no}) = \varphi = V_T \ln \frac{N_A}{n_i} + V_T \ln \frac{N_D(x_{no})}{n_i} \qquad (14)$$

When the emitter junction is forward bias with $V_a > 0$, the barrier height decreases. It means that the boundary value of x_n changes from x_{no} to a certain new x_n greater than x_{no}. This makes the transition region to be narrower. Hence, a new boundary condition for the doping level on the emitter side arises.

Equations (8), (10), (13) and (14) can be summarized as follows:

I) Assume a given value of $l_n \Rightarrow x_n = x_j - l_n$
II) One can find $E(x)$ at l_n and $l_p = x_p - x_j$ from Eq. (7)
III) Change l_n to get different cases of the electric field distribution.
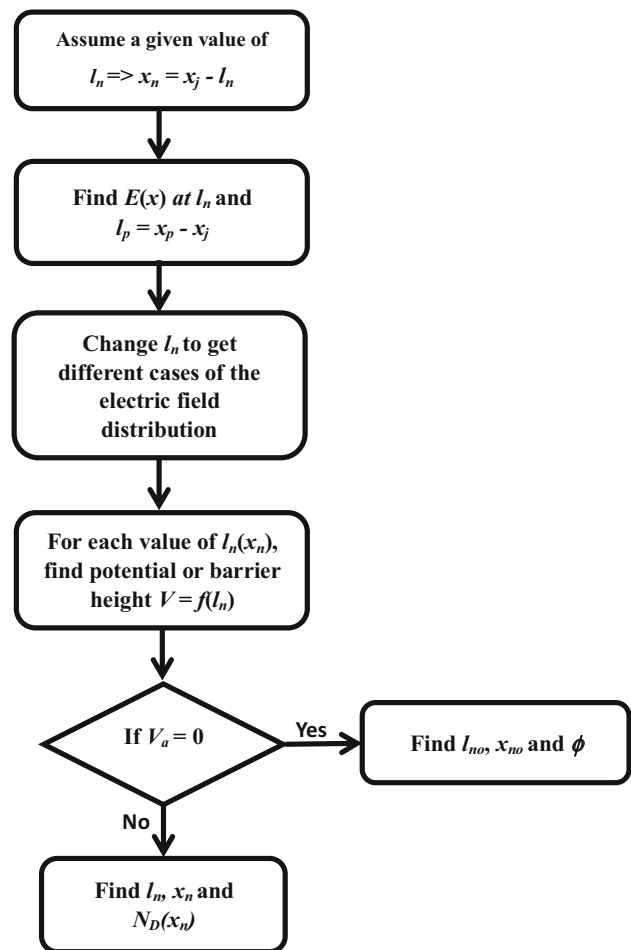
Fig. 4 Flowchart summarizes the steps of calculating l_{no}, x_{no}, l_n and x_n.

IV) For each value of $l_n(x_n)$, one can find the potential or barrier height, i.e., $V_B = f(l_n)$ from Eq. (13)
V) If $V_a = 0$, for each value of l_n, calculate $\varphi(l_n)$ using Eq. (14)
VI) If $V_B(l_n) - \varphi(l_n) = 0$, then $l_n = l_{no}$, and hence $\varphi_o = \varphi(l_{no})$
VII) If $V_a > 0$, by the same way of the previous step, l_n could be found and hence x_n and $N_D(x_n)$.

The last steps are summarized in the flowchart of Fig. 4.

4 Mathematical derivation of the minority carrier concentration

In this section, Poisson's equation is solved to find the boundary limits on both sides of the transition region. The current and continuity equations should be solved to find the profile of minority carriers in the emitter region. Consider the structure in Fig. 2 and assuming low-level injection, the current density of the holes is given by [6],

$$J_p = -qD_p \frac{p}{n_o} \frac{\partial n_o}{\partial x} + q\,\mu_p p E_B - q D_p \frac{\partial p}{\partial x} \qquad (15)$$

The first component of Eq. (15) is the drift component caused by the electric field due to the non-homogeneous profile of the donor concentration. The second component is produced by the electric field due to the band gap narrowing (BGN), where

$$E_B = \frac{2V_T}{n_{ie}} \frac{\partial n_{ie}}{\partial x} \qquad (16)$$

If the BGN effect is neglected, then $n_{ie} = n_i$ and its current component equals zero. Finally, the third part is the diffusion component caused by carrier concentration gradient.

The second equation, to be considered, is the continuity equation which could be written in the form of a partial differential equation, assuming that the minority carriers do not change with time, as follows,

$$0 = -\frac{1}{q} \frac{\partial J_p}{\partial x} - U(p, n) \qquad (17)$$

Then, differentiating Eq. (15) with respect to distance leads to,

$$\frac{1}{q} \frac{\partial J_p}{\partial x} = f_1(x)\,p + f_2(x)\,\frac{\partial p}{\partial x} - D_p \frac{\partial^2 p}{\partial x^2} \qquad (18)$$

where

$$f_1(x) = \frac{\partial}{\partial x} \left[2D_p \frac{1}{n_{ie}} \frac{\partial n_{ie}}{\partial x} - D_p \frac{1}{n_o} \frac{\partial n_o}{\partial x} \right] \qquad (19)$$

and

$$f_2(x) = 2D_p \frac{1}{n_{ie}} \frac{\partial n_{ie}}{\partial x} - D_p \frac{1}{n_o} \frac{\partial n_o}{\partial x} - \frac{\partial D_p}{\partial x} \qquad (20)$$

Now, substitute Eq. (18) in (17), one gets,

$$-D_p \frac{\partial^2 p}{\partial x^2} + f_2(x) \frac{\partial p}{\partial x} + f_1(x)p = -U(p, n) \qquad (21)$$

Combining the SRH and Auger mechanisms, the recombination term $U(p, n)$ could be written as,

$$U(p, n) = N_t C_n C_p \frac{pn - n_i^2}{C_n(n + n_1) + C_p(p + p_1)} + C_A n_0^2(p - p_0) \qquad (22)$$

Assume quasi-equilibrium and $n_0 \gg p_o$ in the n-type emitter, then the recombination term could be simplified to,

$$U(p, n) \approx f_3(x)(p - p_o) \qquad (23)$$

where

$$f_3(x) = C_p N_t + C_A n_0^2 \qquad (24)$$

Substituting Eq. (23) in (21), one obtains,

$$-D_p \frac{\partial^2 p}{\partial x^2} + f_2(x) \frac{\partial p}{\partial x} + [f_1(x) + f_3(x)]\, p = f_3(x) p_o \qquad (25)$$

Since the emitter is a heavily doped semiconductor, it is verified numerically that the term $(f_3(x) p_o)$ can be neglected, and then Eq. (25) becomes,

$$\frac{\partial^2 p}{\partial x^2} - f_5(x) \frac{\partial p}{\partial x} - f_6(x)p = 0 \qquad (26)$$

where

$$f_5(x) = \frac{2}{n_{ie}} \frac{\partial n_{ie}}{\partial x} - \frac{1}{n_o} \frac{\partial n_o}{\partial x} - \frac{1}{D_P} \frac{\partial D_p}{\partial x} \qquad (27)$$

and

$$f_6(x) = \frac{1}{D_P} \frac{\partial}{\partial x} \left[D_P \left(\frac{2}{n_{ie}} \frac{\partial n_{ie}}{\partial x} - \frac{1}{n_o} \frac{\partial n_o}{\partial x} \right) \right] + \frac{C_A n_o^2}{D_P} + \frac{C_p N_t}{D_p} \qquad (28)$$

where N_t is the concentration of recombination center, and it can be expressed as,

$$C_p N_t = C_p N_{to} \left(1 + \left(\frac{N_D}{N_{Dr}} \right)^{\alpha_t} \right) = \frac{1}{\tau_L} \left(1 + \left(\frac{N_D}{N_{Dr}} \right)^{\alpha_t} \right) \qquad (29)$$

where α_t and N_{Dr} are certain parameters to describe N_t. The numerical values of these parameters are chosen to be $\alpha_t = 0.5$, $N_{Dr} = 10^{16}\ cm^{-3}$ and $\tau_L = 1/(C_p N_{to}) = 10\ \mu s$. Similar values are found in the literature ($\alpha_t = 1$, $N_{Dr} = 10^{17}\ cm^{-3}$ and $\tau_L = 10\ \mu s$) [30].

Equation (26) is a second-order differential equation. Two boundary conditions are needed to solve this differential equation; they are:

(i) at $x = 0$, $p = 0$ which means a metallic contact; and
(ii) at $x = x_n$, $p = \Delta p = \frac{n_i^2}{(N_D(x_n) - N_A)} \left(e^{V_a/V_T} - 1 \right)$

A MATLAB program is built to evaluate the analytical model numerically. The profile of minority carriers $p(x)$ and its derivative $\frac{\partial p}{\partial x}$ are found as output from the program. Both $p(x)$ and $\frac{\partial p}{\partial x}$ are necessary to study the behavior of the emitter after calculating the current density at any applied voltage. The hole current is calculated from Eq. (15). The total current

is the hole current at $x = x_n$. Furthermore, the saturation current density is extracted by fitting the simulated current–voltage characteristic using,

$$J = J_o \left(e^{V_a/V_T} - 1 \right) \tag{30}$$

5 Effect of polycrystalline layer

The polysilicon layer is heavily doped with constant donor concentration equals to the surface concentrations N_S of the single layer. The poly-layer is deposited over the single layer. The dopants are diffused from the poly- to the single layer and acts as a diffusion source for the single-crystal emitter layer. The depth of the junction depends on the diffusion temperature and time. The doping concentration in the single layer is described by complementary error function or Gaussian function or any measured profile.

The polysilicon layer is modeled as a mono-silicon layer with a homogeneous profile $N_D(x) = N_S$. The lifetime has an effective value in the polysilicon (τ_{poly}). The interfacial layer contains additional recombination centers following the oxygen atom distribution at the interface, and these recombination centers could be modeled as a Gaussian distribution

$$N_t(x) = N_{to} \exp\left(-\frac{(x - x_{\text{poly}})^2}{2\sigma^2} \right) \tag{31}$$

where σ_c is the capture cross section, N_{to} is the trap density at the interface, and σ is the standard deviation of the trap distribution. This results in an additional recombination lifetime τ_i that can be expressed by:

$$\tau_i(x) = \frac{1}{\sigma_c V_{th} N_t(x)} \tag{32}$$

where V_{th} is the thermal velocity (typically $= 10^7$ cm/s). Values of the recombination parameters could be in the range: $\sigma_c = 10^{-17} \text{cm}^2$, $N_{to} = 10^{17}$ cm^{-3} and $\sigma = 10$ nm [31].

The interface lifetime τ_i is combined to the poly-lifetime in the poly-layer and the single lifetime in the single layer as,

$$\frac{1}{\tau_{eff}(x)} = \frac{1}{\tau_i(x)} + \frac{1}{\tau_{\text{poly}}}, \quad 0 < x < x_{\text{poly}} \tag{33}$$

$$\frac{1}{\tau_{eff}(x)} = \frac{1}{\tau_i(x)} + \frac{1}{\tau_{\text{single}}}, \quad x_{\text{poly}} < x < x_n \tag{34}$$

The term τ_{poly} in Eq. (33) is modified before combining it to τ_i as will be explained. The modification of τ_{poly} comes from the effect of the oxide layer as will be discussed.

In addition to the modification of the lifetime of minority carriers, the interfacial layer constitutes a potential energy barrier for their flow. The schematic distribution of holes
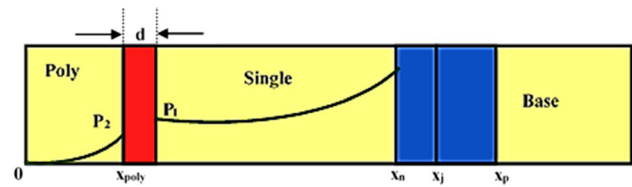
Fig. 5 Hole distribution in the polysilicon emitter

injected in the emitter is shown in Fig. 5. The potential barrier of the interfacial layer causes the hole concentration to be reduced from p_1 at the mono-silicon edge to p_2 at the polysilicon edge of the i-layer.

The tunneling probability of holes across the i-layer could be given by,

$$P_T \approx \exp\left(-d\sqrt{V_{ox}} \right) \tag{35}$$

where d is the interface layer thickness in Angstrom and V_{ox} is the tunneling barrier height. V_{ox} is typically in the range of 1 V [15]. Holes cross the barrier also by thermionic emission. The thermionic emission current is given by,

$$J_{th} = q p_1 V_{th} \exp\left(-\frac{V_{ox}}{V_T} \right) \tag{36}$$

The total hole current at x_{poly} can be expressed by,

$$J_p = q D_p \frac{p_2}{l_p} \tag{37}$$

where l_p is the diffusion length of holes in the poly-layer. The tunneling J_T current has the form,

$$J_T = q (p_1 - p_2) V_{th} P_T \tag{38}$$

The total hole current crossing i-layer is then,

$$J_{\text{tot}} = J_{th} + J_T = q p_1 V_{th} \left(P_T + \exp\left(-\frac{V_{ox}}{V_T} \right) \right) - q p_2 V_{th} \tag{39}$$

Assuming negligible recombination in the i-layer, then $J_p = J_{\text{tot}}$, it follows that the recombined thermionic emission tunneling probability α_{tt} can be put in the form,

$$\alpha_{tt} = \frac{p_2}{p_1} = \frac{\frac{l_p V_{th}}{D_p} \left(P_T + \exp\left(-\frac{V_{ox}}{V_T} \right) \right)}{1 + \frac{l_p V_{th}}{D_p} P_T} \tag{40}$$

Then J_p can be expressed by,

$$J_p = \frac{q D_p p_1 \alpha_{tt}}{L_p} = \frac{q D_p p_1}{\sqrt{D_{\text{poly}}(\tau_{\text{poly}}/\alpha_{tt}^2)}}$$

The effect of the barrier can be formally modeled by defining a new minority carrier lifetime in the polysilicon layer such that,

$$\tau_{\text{polynew}} = \frac{\tau_{\text{poly}}}{\alpha_{tt}^2} \qquad (41)$$

In addition, x_{poly} must be formally extended to $x_{\text{poly}} = (x_{\text{poly}}/\alpha_{tt})$ since the diffusion length will be extended by $(1/\alpha_{tt})$ to preserve the shape of the minority carrier distribution in the polysilicon region. With this formation of the i-layer, the solution domain is reduced to only two regions, namely the mono-silicon layer and the formally new polysilicon layer. In both regions, the minority carrier differential equation is directly applicable.

Now, τ_{poly} will be replaced by τ_{polynew} in Eq. (33). It becomes

$$\frac{1}{\tau_{eff}(x)} = \frac{1}{\tau_i(x)} + \frac{1}{\tau_{\text{polynew}}} \qquad (42)$$

6 Results and discussion

In this section, the results from the developed program under MATLAB are presented. These results include l_n and l_p as a function of potential barrier V_B. Also, the $J–V$ characteristic versus the applied voltage V_a is introduced. Various effects of the design parameters on the emitter properties considering the saturation current density are studied. These include the polysilicon thickness xpoly and doping, background doping and oxide thickness according to the variation of the interface anneal temperature.

6.1 l_n and l_p as a function of potential barrier V_B

Figure 6 shows the variation of l_n and l_p with the potential barrier V_B. It can be depicted from the figure that $l_n < l_p$ due to using the complementary error function profile. Also, it is clear that l_n varies slightly with barrier height V_B. This is because V_B decreases when the p–n junction is forward biased. Thus, the transition regions l_n and l_p decrease.

6.2 $J–V$ characteristics versus the applied voltage V_a

The $J–V$ characteristics are shown in Fig. 7. The best exponential fitting describing the curve is:

$$J_p = 3.4 \times 10^{-12} \exp(38.7\, V_a) \qquad (43)$$

From Eq. (43), the reverse saturation current density J_{po} equals to 3.4×10^{-12} A/cm². If the injected hole current in the emitter decreases, the transistor injection efficiency
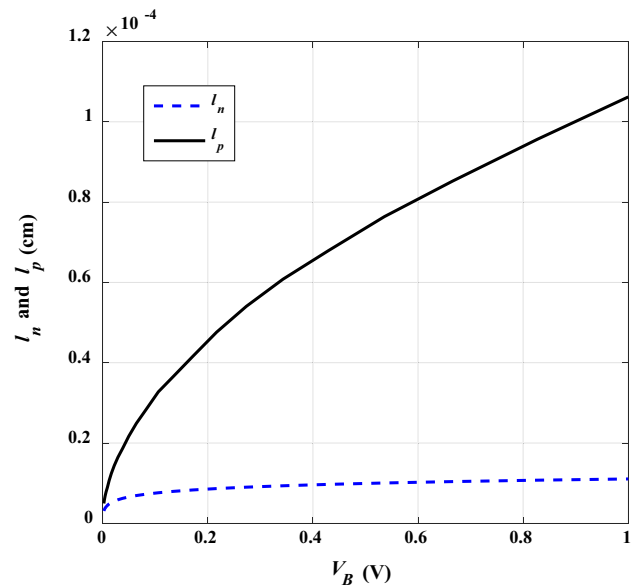
Fig. 6 l_n and l_p as a function of potential barrier V_B with $N_A = 10^{15}$ cm⁻³, $Ns = 10^{17}$ cm⁻³ and diffusion time 1 h
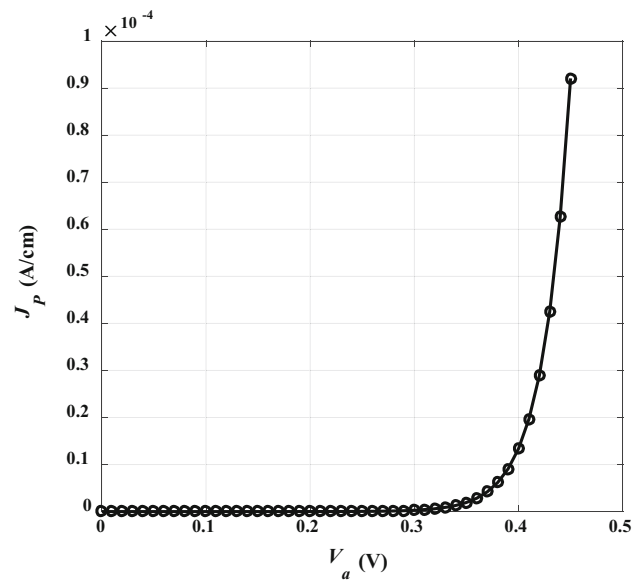
Fig. 7 $J–V$ characteristic with $N_A = 10^{18}$ cm⁻³, $Ns = 10^{20}$ cm⁻³ and diffusion time 1 h

increases. As a result, the amplification factor increases. Thus, the transistor designer aims to reduce J_{po}.

6.3 Effect of design parameters on J_{po}

Firstly, we take the doping profile from an experimental case study [28] to compare the simulated profiles. The process parameters such as diffusivity constant [32], temperature and diffusion time are selected and taken the same for the Gaussian and erfc distributions. Figure 8 shows the simulated profiles for the Gaussian and erfc distributions vs. the
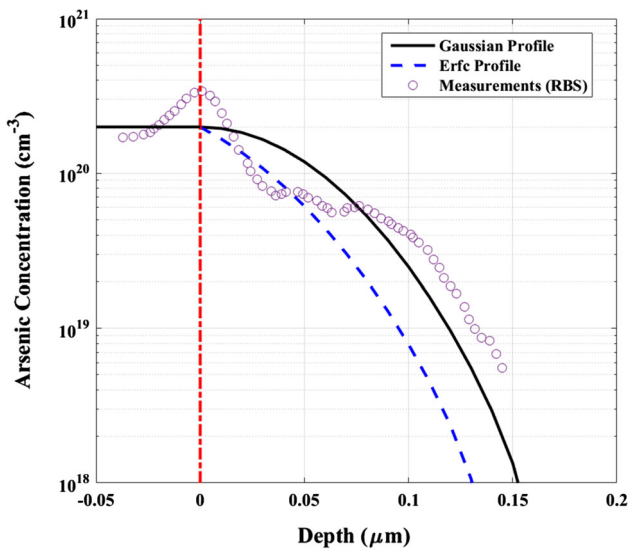
Fig. 8 Simulated As doping profiles vs. experimental profile (T =1000 °C, and diffusion time 0.5 h)

Fig. 9 Effect of x_{poly} and Gaussian function profile with different N_S

Fig. 10 Effect of background concentration N_A on J_{po} at $N_S = 10^{20}$ cm^{-3} and $x_{poly} = 0.4$ μm

chemical concentration which is measured using Rutherford backscattering (RBS) [28]. The average doping in the polysilicon region is taken to be 2×10^{20} cm^{-3}. The figure indicates that the Gaussian distribution is more realistic than the erfc function for this case study. Consequently, Gaussian distribution function will be used in the following simulations.

Figure 9 reflects the effect of poly-layer thickness x_{poly} on J_{po}. The poly-layer thickness x_{poly} changes from zero to 0.7 μm at two different values of surface concentration (2×10^{20} cm^{-3} and 3.3×10^{19} cm^{-3}) as in [28]. From the figure, J_{po} decreases with increasing x_{poly} until it is nearly saturated. Also the measured saturation current density is shown [28]. These results represent a validation of the trends of the proposed model.

The effect of background concentration is also studied. The results are illustrated in Fig. 10. It can be depicted that N_A has the same effect as N_S on J_{po} where increasing N_A tends to decreasing J_{po}.

In the following analysis, experimental results from [11] are considered in which an interface anneal was carried out after polysilicon deposition. It is evident, based on measurements, that the base current increase significantly as the interface anneal temperature is increased from 800 to 1100 °C. These results were correlated with experimental observations which showed that an interfacial oxide was present and broke up as the interface anneal temperature was increased [11].

The simulation is carried out as follows. The doping profile is checked to be consistent with that of the measured data [15] for an active emitter area of 20 μm × 18 μm. The oxide thickness is taken as a fitting parameter to match the experimental data of the saturation current. In doing so, the oxide thickness was firstly taken to be 15 Å. This value of oxide thickness gives $I_{po} = 3 \times 10^{-20}$ A. The thickness is found to be less for higher temperature as expected. The oxide thickness is varied from 15 Å (at $T = 800$ °C) to 8 Å (at $T = 1100$ °C which corresponds to maximum oxide break up). The simulated results along with measurements are presented in Fig. 11 showing good agreement between simulations and measurements.
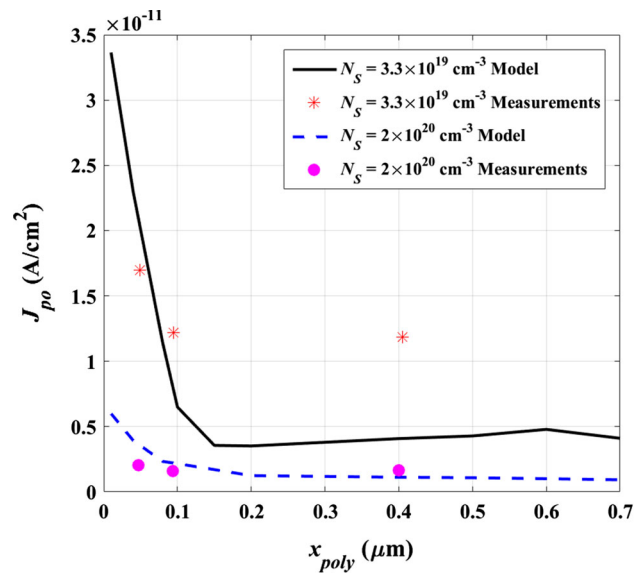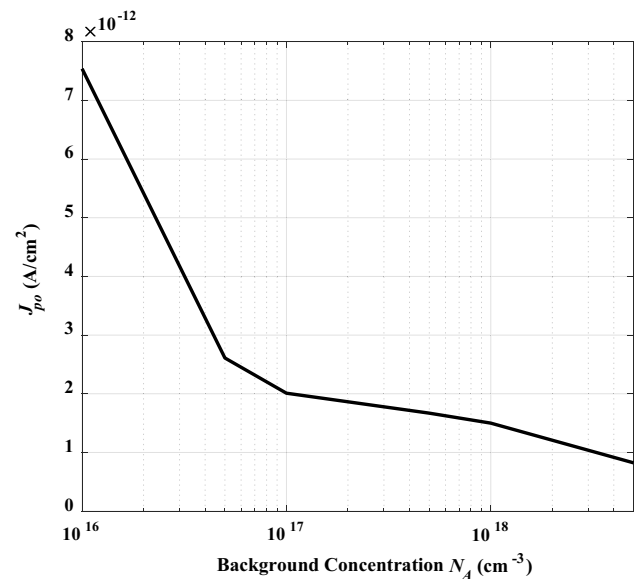
From the simulations carried out in this section, we can conclude with the following remarks. In order to enhance the performance of the polysilicon emitter, it is required to decrease the saturation current as possible as we can. So, it
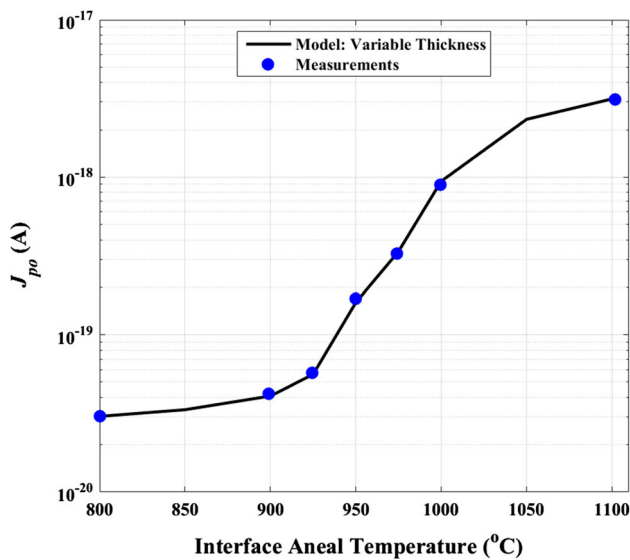
Fig. 11 Effect of interface anneal temperature on I_{po}

is recommended to increase the doping concentration in the poly-emitter, or increasing the thickness of the poly-layer. Also, there should be some treatment to control the oxide thickness as results show its important encounter in the performance. The presented results can be used to optimize the performance of the polysilicon emitter. It may be pointed out that the presented numerical model is also applicable to any mono-crystal emitter with any arbitrary doping profile.

It can be concluded from these simulations that accurate numerical simulation capabilities are essential to optimize this type of emitter. The presented approach enables the prediction of the performance of this complicated contact before its fabrication.

7 Conclusion

The polysilicon emitter has been modeled using a numerical and analytical approach. A general physical model has been developed which takes into account the effect of the technological parameters on the electrical characteristics of the emitter. The semiconductor equations have been applied to the different regions of the polysilicon emitter to set up the analytical system. High doping effects on the semiconductor parameters have been included. The system of equations has been solved numerically to calculate the I–V characteristics of the emitter. To realize this solution, a simulation program has been developed under the MATLAB environment. The accuracy of the solution is confirmed by comparing the numerical solution with published experimental results. Many simulations have been executed to study the effect of the physical parameters on the emitter performance.

It was found that the saturation current could be decreased by many factors: increasing the polysilicon doping and/or thickness, increasing the background concentration and proper treatment of the oxide layer. These physically based simulation results are essential to optimize this type of contact because they enable the prediction of the performance of this complicated contact. Moreover, the presented model could be easily modified to be applied to similar structures like those encountered in solar cell applications.

References

1. Hutchinson, C., Frank, M., Negus, K.: Silicon Bipolar 12 GHz down converter for satellite receivers. In: Proceedings of the IEEE Bipolar/BiCMOS Circuits and Technology Meeting, (BCTM) 198–201 (1995)
2. Nakamura, T., Nishizawa, H.: Recent progress in bipolar transistor technology. IEEE Trans. Electron Devices **42**(3), 390–398 (1995)
3. Wagner, C., Schuster, J., Gessner, T.: Empirical transport model of strained CNT transistors used for sensor applications. J. Comput. Electron. **15**(3), 881–890 (2016)
4. Sedra, A.S., Smith, K.C.: Microelectronic Circuits. Oxford University Press, New York (2014)
5. Warnock, J.D.: Silicon bipolar device structures for digital applications: technology trends and future directions. IEEE Trans. Electron Devices **42**(3), 377–389 (1995)
6. Ning, T.H.: History and future perspective of the modern silicon bipolar transistor. IEEE Trans. Electron Devices **48**(11), 2485–2491 (2001)
7. Ning, T.H., Isaac, R.D., Solomon, P.M., Tang, D.L., Yu, H.N., Feth, G.C., Wiedmann, S.K.: Self-aligned bipolar transistors for high-performance and low-power-delay VLSI. IEEE Trans. Electron Devices **28**(9), 1010–1013 (1981)
8. De Graaff, H.C., De Groot, J.G.: The SIS tunnel emitter: a theory for emitters with thin interface layers. IEEE Trans. Electron Devices **26**(11), 1771–1776 (1979)
9. Ning, T.H., Isaac, R.D.: Effect of emitter contact on current gain of silicon bipolar devices. IEEE Trans. Electron Devices **27**(11), 2051–2055 (1980)
10. Neugroschel, A., Arienzo, M.A.U.R.I.Z.I.O., Komem, Y., Isaac, R.D.: Experimental study of the minority-carrier transport at the polysilicon–monosilicon interface. IEEE Trans. Electron Devices **32**(4), 807–816 (1985)
11. Wolstenholme, G.R., Jorgensen, N., Ashburn, P., Booker, G.R.: An investigation of the thermal stability of the interfacial oxide in polycrystalline silicon emitter bipolar transistors by comparing device results with high-resolution electron microscopy observations. J. Appl. Phys. **61**(1), 225–233 (1987)
12. Special Issue on Bipolar and BiCMOS/CMOS Devices and Technologies. IEEE Trans. Electron Devices, 42, (1995)
13. Sakalas, P., Schroter, M., Zirath, H.: mm-Wave noise modeling in advanced SiGe and InP HBTs. J. Comput. Electron. **14**(1), 62–71 (2015)
14. Peibst, R., Römer, U., Larionova, Y., Rienäcker, M., Merkle, A., Folchert, N., Tetzlaff, D.: Working principle of carrier selective poly-Si/c-Si junctions: Is tunnelling the whole story? Solar Energy Mater. Solar Cells **158**, 60–67 (2016)
15. Post, I.R., Ashburn, P., Wolstenholme, G.R.: Polysilicon emitters for bipolar transistors: a review and re-evaluation of theory and experiment. IEEE Trans. Electron Devices **39**(7), 1717–1731 (1992)

16. Ajuria, S.A., Gan, C.H., Noel, J.A., Reif, L.R.: Quantitative correlations between the performance of polysilicon emitter transistors and the evolution of polysilicon/silicon interfacial oxides upon annealing. IEEE Trans. Electron Devices **39**(6), 1420–1427 (1992)

17. Loiko, K. V.: A Model for Minority Carrier Mobility in Polysilicon Emitters. scientific J. KubSAU, **90**(6), (2013)

18. Ng, C.C., Yang, E.S.: A thermionic-diffusion model of polysilicon emitter. In: Proceedings IEEE IEDM Technical Digest, 32–35 (1986)

19. Jalali, B., Yang, E.S.: A general model for minority carrier transport in polysilicon emitters. J. Solid State Electron. **32**(4), 323–327 (1989)

20. Yu, Z., Ricco, B., Dutton, R.W.: A comprehensive analytical and numerical model of polysilicon emitter contacts in bipolar transistors. IEEE Trans. Electron Devices **31**(6), 773–784 (1984)

21. Eltoukhy, A.A., Roulston, D.J.: The role of the interfacial layer in polysilicon emitter bipolar transistors. IEEE Trans. Electron Devices **29**(12), 1862–1869 (1982)

22. Zouari, A., Arab, A.B.: Analytical model and current gain enhancement of polysilicon-emitter contact bipolar transistors. IEEE Trans. Electron Devices **55**(11), 3214–3220 (2008)

23. Jin, H.Y., Zhang, L.C., Gao, Y.Z., Ye, H.F.: An equivalent heterojunction-like model for polysilicon emitter bipolar transistor. J. Solid State Electron. **47**(10), 1719–1727 (2003)

24. Jiang, X.L., Guo, W.L., Zhang, Y.M.: A unified model of a poly-Si emitter transistor for various emitter structures. J. Semicond. Sci. Technol. **9**(5), 1117–1125 (1994)

25. Suzuki, K.: Unified minority-carrier transport equation for polysilicon or heteromaterial emitter contact bipolar transistors. IEEE Trans. Electron Devices **38**(8), 1868–1877 (1991)

26. Rinaldi, N.F.: On the modeling of polysilicon emitter bipolar transistors. IEEE Trans. Electron Devices **44**(3), 395–403 (1997)

27. Ma, P., Zhang, L., Zhao, B., Wang, Y.: An analytical model for determining carrier transport mechanism of polysilicon emitter bipolar transistors. IEEE Trans. Electron Devices **42**(10), 1789–1797 (1995)

28. Patton, G.L., Bravman, J.C., Plummer, J.D.: Physics, technology, and modeling of polysilicon emitter contacts for VLSI bipolar transistors. IEEE Trans. Electron Devices **33**(11), 1754–1768 (1986)

29. Ashburn P., Soerowirdjo B.: Comparison of experimental and theoretical results on polysilicon emitter bipolar transistors. In: IEEE Transactions Electron Devices, ED-31, 853–860 (1984)

30. Law, M.E., Solley, E., Liang, M., Burk, D.E.: Self-consistent model of minority-carrier lifetime, diffusion length, and mobility. IEEE Electron Device Lett. **12**(8), 401–403 (1991)

31. Sentaurus, TCAD. "Manuals" Synopsys Inc., Mountain View, CA 94043 (2009)

32. Neudeck, G., Pierret, R.F., Jaeger, R.W.: Introduction to microelectronic fabrication (1988)